Hindawi Publishing Corporation
Journal of Nanomaterials
Volume 2014, Article ID 914847, 8 pages
http://dx.doi.org/10.1155/2014/914847

Research Article

Ta_2O_5 Nanowires, Nanotubes, and Ta_2O_5/SiO_2 Core-Shelled Structures: From Growth to Material Characterization

Hsu-Sheng Tsai, Tsung-Ying Yang, Mu-Tung Chang, Li-Jen Chou, and Yu-Lun Chueh

Department of Materials Science and Engineering, National Tsing Hua University, Hsinchu 300, Taiwan

Correspondence should be addressed to Yu-Lun Chueh; ylchueh@mx.nthu.edu.tw

Received 27 December 2013; Accepted 30 January 2014; Published 24 March 2014

Academic Editor: Wenjie Mai

One-dimensional polycrystalline Ta_2O_5 nanostructures are synthesized by the annealing of the SiO_2 nanowires at 950°C in a reductive Ta vapor ambiance. The formation mechanism of Ta_2O_5 nanostructures is discussed and illustrated in detail. The nucleation and grain growth of Ta_2O_5 crystals were investigated during the formation of the SiO_2/Ta_2O_5 core-shelled structures. The diffusion-controlled growth is suggested to be the rate-determining step for the diffusion of the Ta atoms through the ash layer to react with O atoms and substitute Si atoms.

1. Introduction

One-dimensional nanomaterials such as nanowires, nanorods, nanobelts, and nanotubes are much attractive owing to their unique optical, electronic, and mechanical properties [1–5]. Among them, the metal oxides so-called functional materials, such as MgO [6], ZnO [7], SnO_2 [8], In_2O_3 [9], Ga_2O_3 [10], WO_3 [11], and Ta_2O_5 [12], are aimed to be extensively studied. The growth methods, including vapor-solid growth (VS) [7], vapor-liquid-solid growth (VLS) [13], oxide-assisted growth (OAG) [14], solution-based growth [15], solution-liquid-solid growth (SLS) [16], and template-assisted growth [17], have been adopted and reported to synthesize these one-dimensional nanostructures. Beyond synthesis, these kinds of materials are applied in electronic devices like field effect transistor [18–20].

So far, tantalum pentoxide (Ta_2O_5) has been a hot subject both in the industry and the academic world. It is the best candidate for the dielectric materials used in the next generation dynamic random access memory (DRAM) due to its high dielectric constant. In addition, the Ta_2O_5 applied to optical waveguide [21], antireflective coating layer [22], anticorrosion layer [23], chemical or biological sensitive layer [24, 25], and photocatalyst [26] possesses high refractive index, high chemical stability, and high temperature piezoelectric property. In Ta-O system, the Ta_2O_5 can be categorized into two equilibrium phases, including α-Ta_2O_5 at high temperature and β-Ta_2O_5 at low temperature, respectively. Besides, Fukumoto and Miwa claimed that hexagonal δ-Ta_2O_5 may exist through the first principle ultrasoft pseudopotential calculation [27]. Even if the amorphous and polycrystalline Ta_2O_5 thin films have been widely studied and synthesized, nevertheless, its one-dimensional nanostructures are still lacking in reports.

In this letter, we demonstrate how to fabricate the Ta_2O_5/SiO_2 core-shelled structures and the Ta_2O_5 NWs as well as the Ta_2O_5 nanotube *via* the annealing of SiO_2 NWs in a Ta reductive ambiance. The main idea is based on the lower heat formation of Ta_2O_5, which can be formed by the oxidation of Ta and the reduction of SiO_2 at the same time. The growth mechanism of SiO_2/Ta_2O_5 core-shelled structures was constructed and investigated. On the other hand, we first illustrated the electronic structure of Ta_2O_5/SiO_2 core-shelled nanowire by using the electron energy loss spectroscopy (EELS). A couple of sequential experiments under different annealing conditions were performed to realize the growth mechanisms.

2. Experiments

The single crystal (100) Si (1–30 Ω-cm) wafers were cleaned by the standard RCA procedures. The Si substrate capped by

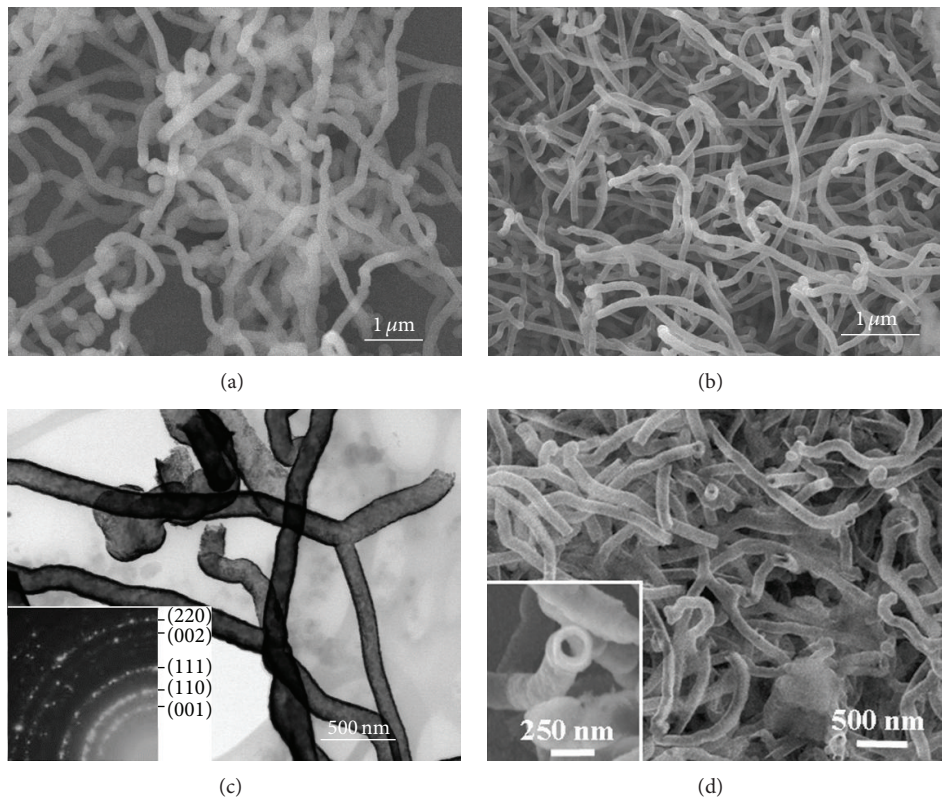

Figure 1: (a) A top-view SEM image of SiO_2 nanowires grown at 1150°C for 2 hours in a N_2 ambient. (b) A top-view SEM image of polycrystalline Ta_2O_5/SiO_2 core-shelled nanowires synthesized by annealing SiO_2 nanowires in a reductive Ta vapor ambient at 950°C for 4 hours. (c) The corresponding TEM image of (b) with the selected area diffraction (SAD) in the lower inset. (d) The SEM image of Ta_2O_5 nanotubes after dipping into the dilute HF solution with the magnified SEM image in the lower inset.

a 2 nm thick Au layer deposited at a pressure of 5×10^{-6} Torr with a deposition rate of 0.01 nm/sec was annealed in a horizontal furnace at 1150°C for 2 hours in a N_2 ambiance to grow SiO_2 nanowires. The SiO_2 nanowires produced by our approach were transferred into a Ta filament heating chamber where the Ta atoms were constantly vaporized as the supplementary source for annealing at a pressure $< 1 \times 10^{-6}$ Torr at 950°C for 1–32 hours. The core-shelled structures of SiO_2 nanowires surrounded by a Ta_2O_5 layer could be synthesized. In addition, the Ta_2O_5 nanotube could be formed by dipping the Ta_2O_5/SiO_2 core-shelled nanowires in diluted HF solution ($HF : H_2O = 1 : 50$) to remove the inner SiO_2 nanowire. The wide angle X-ray diffraction spectrometer (Shimadzu) and the grazing incidence X-ray diffraction spectrometer (GIXRD, MAC) with a fixed incident angle of 0.5° were used to identify the phases of the nanowires. Field-emission transmission electron microscope (JEM-3000F, operated at 300 kV with point-to-point resolution of 0.17 nm) equipped with an energy dispersion spectrometer (EDS) was used to obtain the information of the nanostructures and the chemical compositions. The surface morphology examined by a field-emission scanning electron microscope (JSM-6500F) was operated at 15 kV. In TEM, the electronic structure of a single NW can be investigated by EELS. The electronic structure in the valence band can be qualitatively identified from the fine structures in the ionization edges. All of the raw EELS spectra were calibrated in the relative energy position by zero-loss peak and then subtracted by power law to remove the background signal generated by plural-scattering events. After recalibration of energy positions and removal of multiple scattering effects, EELS spectra were deconvoluted by the plasma and the low loss spectra by Fourier-log method to obtain the true single-scattering spectrum.

3. Results and Discussion

Figure 1(a) shows the SEM image of SiO_2 NWs synthesized by annealing the Au thin layer at 1150°C for 2 hours in a N_2 ambiance. The SiO_2 NWs with diameter of about 200 nm are uniformly distributed over all the substrate. However, we can obviously find out that all the SiO_2 NWs are almost wrinkled and tangled together. After annealing in a Ta reductive ambiance for 4 hours, the morphology is still identical, as shown in Figure 1(b). The corresponding TEM image is shown in Figure 1(c) where the selected area diffraction (SAD) is identified and shown in the inset. This SAD analysis unambiguously gives us an evidence of the SiO_2 NWs surrounded by Ta_2O_5 uniformly. Moreover, the morphology of Ta_2O_5/SiO_2 core-shelled structures can be alternated by tuning the morphology of SiO_2 NWs. For the

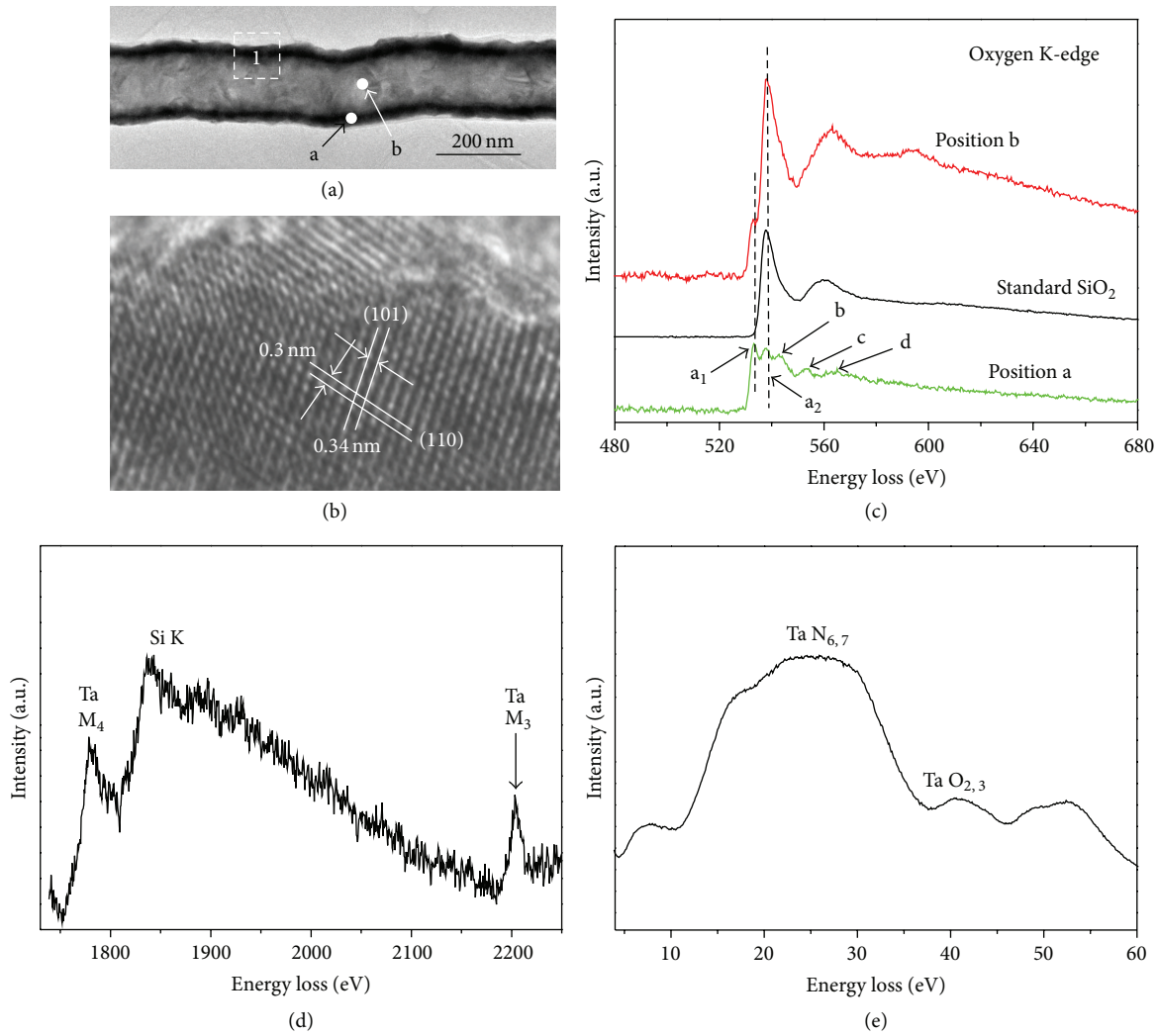

FIGURE 2: (a) A TEM image of the Ta_2O_5/SiO_2 core-shelled structures formed by annealing the Si NWs in a Ta ambient for 8 hours. (b) The corresponding HRTEM image taken from the rectangular area marked as 1 of (a). (c) The EELS spectra of oxygen K-edge ELNES recorded from a and b positions of (a) and the as-synthesized SiO_2 NWs. (d), (e) Other EELS spectra of the Ta_2O_5 shell.

present case, the SiO_2 NWs formed by annealing the Au thin layer at high temperature in a N_2 ambiance are almost tangled together so that the core-shelled structures mostly form multijunctions with 9~11 nm thickness of the Ta_2O_5 shell after annealing in a Ta reductive ambiance. Furthermore, the Ta_2O_5 nanotubes can be formed after dipping the sample into the dilute HF solution. An example is shown in Figure 1(d) and the magnified SEM image is also shown in the inset.

The EELS spectrum can give us the information of chemical bonding and relative electron configuration. Figure 2(a) reveals the Ta_2O_5/SiO_2 core-shelled structures formed by annealing the SiO_2 NWs in a Ta ambiance for 8 hours and the corresponding high resolution TEM image taken from a rectangular area marked as 1 in Figure 2(a) is shown in Figure 2(b). The interplanar distances of 0.3 and 0.34 nm, which are consistent with planes of (110) and (101), are indexed. Figure 2(c) shows the three different EELS spectra of oxygen K-edge energy loss near edge fine structure (ELNES) recorded from a and b positions in Figure 2(a) and the as-synthesized SiO_2 NWs. All of the raw data have been calibrated in energy scale by the zero-loss peak and deconvoluted by the low loss region to reduce the multiple-scattering effect. Five peaks were denoted as a_1, a_2, b, c, and d at the positions of 533.1, 537.2, 542.9, 553.6, and 565.3 eV, respectively. The peaks, a_1 and a_2, are derived from the O 2p orbit hybridized with Ta 5d orbit to separate into two symmetry bands identified as the t_{2g} and e_g by ligand-field splitting, for which the term "ligand-field splitting" means the "bare" (ionic) crystal field splitting plus hybridization [28]. The Δd between a_1 and a_2 in present study can be found to be 4.1 eV. The peak b is originated from the oxygen 2p orbit hybridized with the transition metal 6s and 6p orbits, respectively. The peaks c and d resulted from the scattering of the third- and the first-coordinated oxygen with the outgoing or backscattering electrons. Furthermore, the oxygen K-edge ELNES of the core-shelled structures (Ta_2O_5/SiO_2) taken

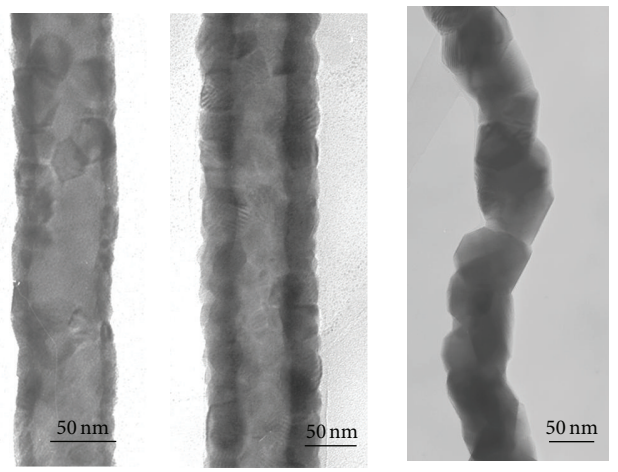

FIGURE 3: (a) The formation process of polycrystalline Ta_2O_5 nanowire nucleation of Ta_2O_5 crystals *via* the reduction of SiO_2. (b) The grain growth of Ta_2O_5. (c) The polycrystalline Ta_2O_5 nanowire formed through the intersection of grains.

from the position b in Figure 2(a), as shown in the upper part of Figure 2(c), is different from the results of position a. In order to make a comparison, the as-synthesized oxygen K-edge ELNES of SiO_2 NWs was acquired as shown in the middle of the Figure 2(c). Obviously, it suggests that the oxygen K-edge ELNES recorded from the position b in Figure 2(c) is superimposed by that of SiO_2 and Ta_2O_5, revealing that the inner is a SiO_2 nanowire surrounded by a uniform coating of Ta_2O_5 shell. Other EELS spectra of the shell shown in Figures 2(d) and 2(e) provide electronic structure of Ta_2O_5 as well. The peaks located at around 2200 eV and 1800 eV correspond to the Ta $3p^{3/2}$ and Ta $3d^{3/2}$, respectively. The peaks of Ta 4s and Ta 5p orbits are also exhibited in the spectrum. Besides, the Si K-edge signal comes from the SiO_2 core.

The heat of formation for transition metal oxides such as HfO_2, TiO_2, and Ta_2O_5 is lower than that of SiO_2 [29], resulting in the reduction of SiO_2 at high annealing temperatures. Oppositely, the reduction of SiO_2 is prohibited if the heat of formation for transition metal oxides is higher than that of SiO_2. The formation of Ta_2O_5 phase is accomplished by the Ta vapor to react with SiO_2 and the oxidation-reduction reaction is given by

$$4Ta + 5SiO_2 \longrightarrow 2Ta_2O_5 + 5Si. \quad (1)$$

According to the thermodynamic calculation, the equilibrium phases of Ta-SiO_2 system are Ta_2O_5 and Ta_2Si in the temperature range from 700 to 1300°C [30]. In our case, the Ta_2Si phase was not formed inside the Ta_2O_5 nanowires examined by the XRD spectra and the TEM diffraction pattern. This result might be attributed to the activation energy for the nucleation of the Ta_2Si phase [31] in the reaction of Ta-Si system, for which Ta atoms are difficult to react with Si atoms at the annealing temperature below 1100°C. Therefore, in our process, the annealing temperature of 950°C would not be high enough for the nucleation of Ta_2Si.

The polycrystalline feature is suggested to be caused by two probable mechanisms: the segregation of Si *via* the grain boundaries of Ta_2O_5 nanowires and the anisotropic reduction along the SiO_2 nanowires. The dislocations, which may be caused by the Si atoms in the substitutional or interstitial sites of the sublattice of Ta_2O_5, can be found inside the grain of Ta_2O_5. The sequential formation mechanisms of the polycrystalline Ta_2O_5 nanowires *via* reduction of SiO_2 nanowires in the Ta vapor ambient are illustrated in Figures 3(a) to 3(c). The Ta_2O_5 nanocrystals first nucleated *via* reducing amorphous outer layer of the SiO_2 nanowires by Ta atoms. The Ta_2O_5 grain growth is through growth of the smaller grains to reduce the grain boundary energy during the continuous shrinking process of the inner SiO_2 nanowires; consequently, the polycrystalline Ta_2O_5 outer shells and Ta_2O_5/SiO_2 core-shelled structures were obtained. As the shrinking process proceeded, the pearl-like string of the polycrystalline Ta_2O_5 nanowires is the final form of the feature.

Figure 4(a) illustrates the TEM image of Ta_2O_5/SiO_2 core-shelled nanowire whose granular morphology of the surface exhibits the sizes of the nanocrystals below 3 nm after annealing for 30 minutes. Figures 4(b) and 4(d) reveal the amorphous-like regions between Ta_2O_5 grains taken from the magnified image of rectangular area in Figure 4(a), respectively. Autocorrelation function (ACF) analysis was used to study the amorphous-like region for realizing whether it is a purely amorphous structure or not. Figures 4(c) and 4(e) illustrate the ACF analytical results, which make a comparison of the square areas of numbers (1) to (25), respectively. The ACF data in Figure 4(c) indicates that fine Ta_2O_5 grains exist in the outer periphery areas of the nanowire and the core region of the nanowire still retains amorphous structure. The lattice fringes shown in Figure 4(e) are

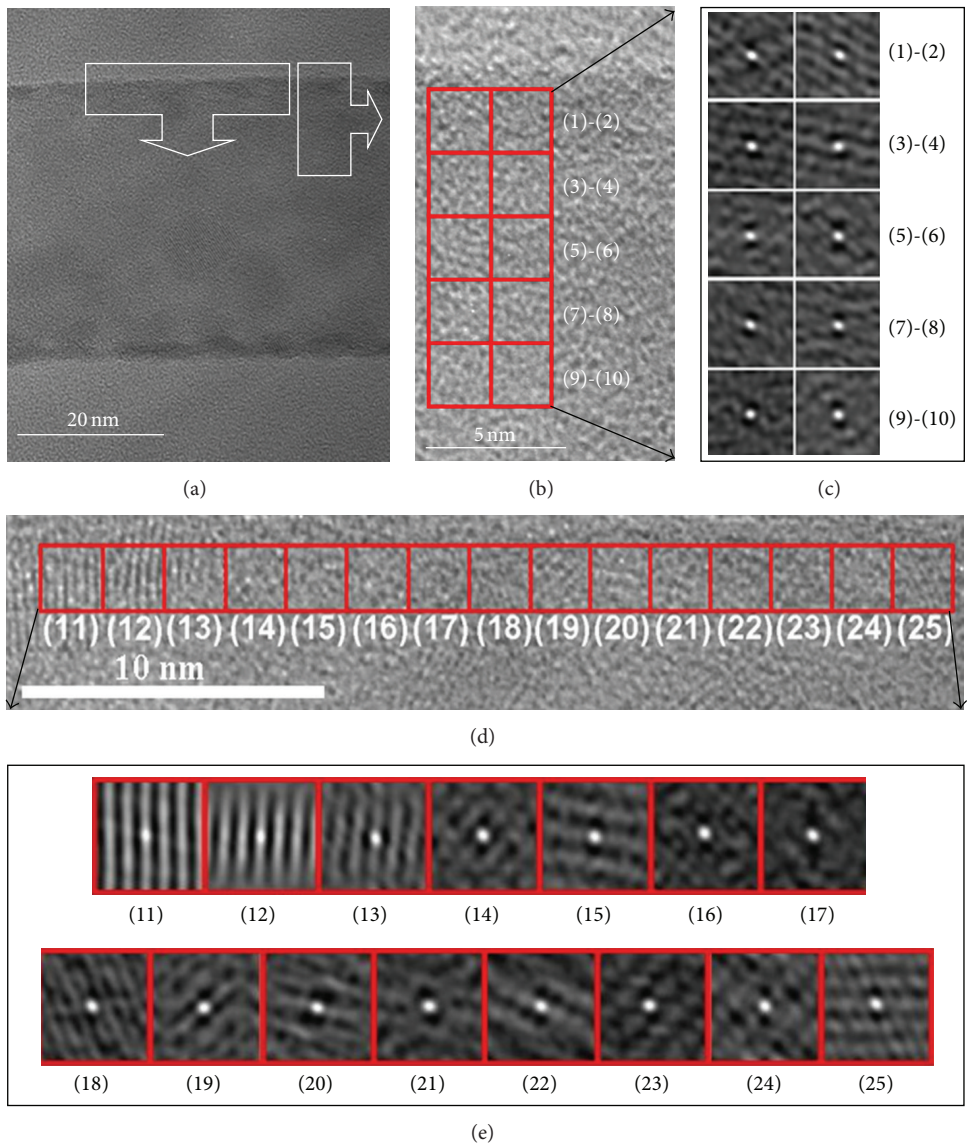

FIGURE 4: (a) A TEM image of a 30-minute annealed Ta_2O_5/SiO_2 core-shelled nanowire. (b) and (d) indicate the magnified TEM image of rectangle area of (a). (c) and (e) indicate the corresponding ACF analysis results of square area numbers (1)~(25) of (b) and (d).

clearly observed in the ACF results, which reveal that the crystal structure in this area should be purely amorphous or very short-range order. The ACF results strongly suggest that there are fine grains in the amorphous-like region and their phases are identified to be Ta_2O_5 by verifying the spacing and angle of plane. The data also indicates that the nearby fine grains tend to orientate in the same direction for reducing the total free energy. The grain growth proceeds *via* an agglomeration mechanism during the annealing process.

Figures 5(a) to 5(e) show TEM images of the SiO_2/Ta_2O_5 core-shelled nanowire formed by annealing the SiO_2 nanowire in the Ta ambient for 1, 2, 4, 8, and 16 hr, respectively. The TEM images indicate that the thickness of Ta_2O_5 shell layer increases and the diameter of SiO_2 core decreases simultaneously with the annealing time. The number of Ta_2O_5 grains decreases while the size increases during the annealing process. This phenomenon also indicates occurrence of agglomeration process during the grain growth. Figure 5(f) shows the relationship between the thickness of Ta_2O_5 shell layer and the annealing time at 950°C. The thickness of Ta_2O_5 shell layer increases since the Ta atoms diffuse through the shell layer and then reduce SiO_2 core layer. The growth rate of Ta_2O_5 shell layer could be dominated by either diffusion or reaction mechanism. As shown in Figure 5(f), the growth rate of Ta_2O_5 shell layer decreases with the annealing time, suggesting that the diffusion through the shell layer would dominate the reduction process. Szekely and Themelis proposed a cylinder [32] growth model, which considers the reaction of a cylinder material B reduced by another material A to form products as given by

$$A + bB \longrightarrow \text{products} \tag{2}$$

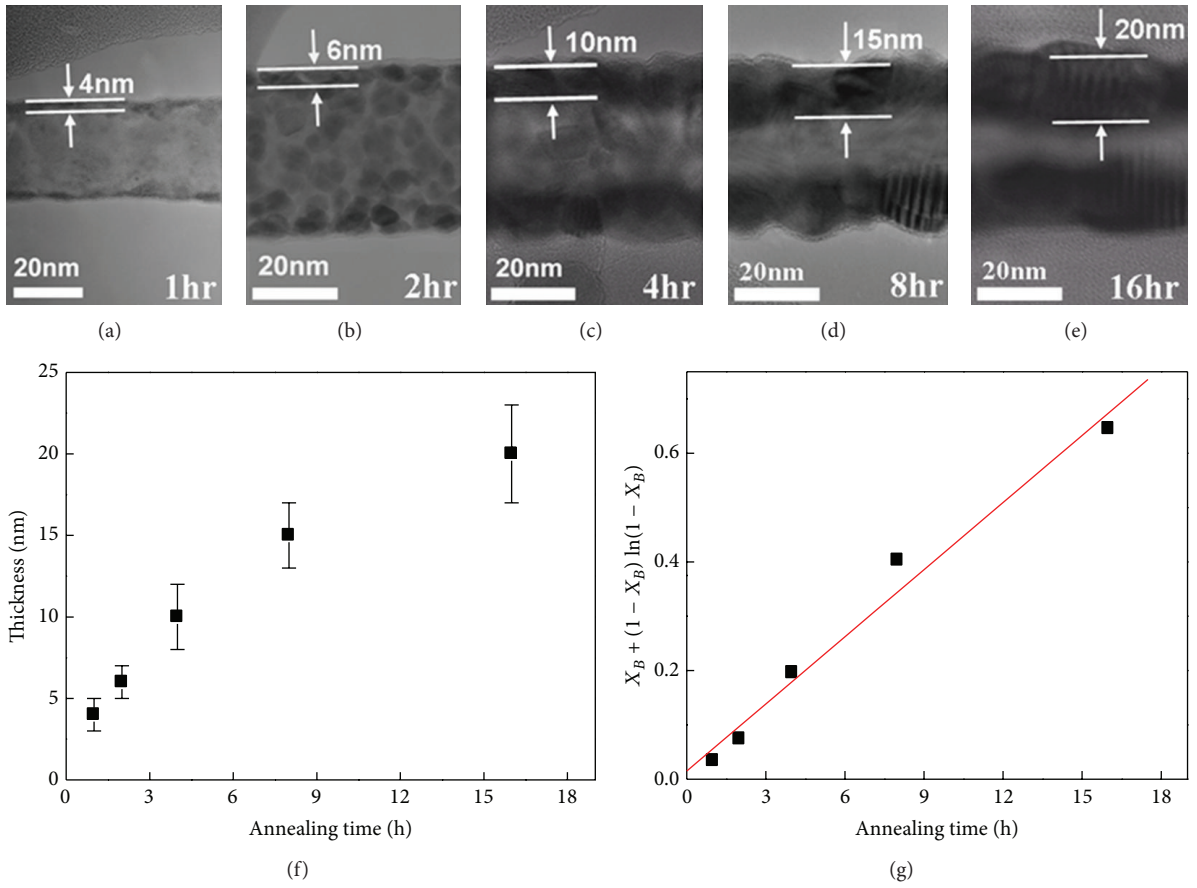

FIGURE 5: (a) to (e) TEM images of Ta_2O_5/SiO_2 core-shelled nanowire formed under different annealing time of 1, 2, 4, 8, and 16 hours, respectively. (f) The annealing time as the function of the thickness of Ta_2O_5 shell layer. (g) The annealing time as the function of $X_B + (1 - X_B)\ln(1 - X_B)$, from (3), with the corresponding fitting line.

$$\frac{t}{\tau} = X_B + (1 - X_B)\ln(1 - X_B) \tag{3}$$

$$\tau = \frac{\rho_B R^2}{6bD_e C_{\mathrm{Ag}}} \tag{4}$$

$$X_B = 1 - \left(\frac{r_c}{R}\right)^2, \tag{5}$$

where t is the reaction time, τ is the complete reaction time, X_B is the mole fraction of B cylinder, ρ_B is the molar density of B cylinder, R is the cylinder radius, b is the equilibrium constant of reaction, D_e is the effective diffusion coefficient of gaseous reactant in the ash layer, C_{Ag} is the concentration of A vapor at cylinder surface, and r_c is the radius of unreacted core, respectively. By applying the growth model, the diameters of SiO_2 nanowires are assumed to be 60 nm and the Ta vapor pressure source is a constant. The corresponding relationship between the value of $X_B + (1 + X_B)\ln(1 - X_B)$ and the annealing time by fitting our experimental data is shown in Figure 5(g). The complete reaction time computed from the fitting line is about 30 hours, which quite matches with the 32 hours for annealing of our experiments.

So far, we can confirm that the growth of the Ta_2O_5/SiO_2 core-shelled nanowires is controlled by diffusion through the ash layer. But the problem, whether Ta atoms or Si atoms are the most effective diffusion species during the reduction process, still needs to be answered. It suggested that the diffusion velocity of Si atoms should be larger than that of Ta atoms. The gradient of the Si concentration between the shell layer and the core causes the higher driving force for diffusion of the Si atoms out of the ash layer. Also, the atomic radius of the Ta (146 pm) is larger than that of the Si (117.6 pm); furthermore, the difference of the electronegativity between the Ta (1.5) and O (3.44) is higher than that of the Si (1.9) and O (3.44). This suggests that the diffusion of the Ta atoms through the Ta_2O_5 shell layer should be more difficult than that of the Si atoms. Consequently, the diffusion of the Ta atoms should be the rate-determining step of the diffusion-controlled growth.

4. Conclusions

Polycrystalline Ta_2O_5 nanostructures including nanowires, nanotubes, and SiO_2/Ta_2O_5 core-shelled nanowires were successfully synthesized *via* annealing of the SiO_2 nanowires at 950°C in a reductive Ta vapor ambiance. The Ta_2O_5 phase was formed from SiO_2 template reduced by Ta and the formation mechanism of Ta_2O_5 nanostructures was discussed.

The sequential investigations of the nucleation and grain growth of the Ta_2O_5 crystals were monitored by the HRTEM during the formation of the SiO_2/Ta_2O_5 core-shell structures. The diffusion-controlled growth is suggested to be the rate-determining step for the diffusion of the Ta atoms through the ash layer to react with the oxygen atoms and replace the Si atoms. This novel synthesis method may provide the solution to produce other functional metal oxides nanostructures for the future applications.

Conflict of Interests

The authors declare that there is no conflict of interests regarding the publication of this paper.

Acknowledgments

The research was supported by the National Science Council through Grant nos. NSC 101-2112-M-007-015-MY3, 101-2218-E-007-009-MY3, 102-2633-M-007-002, and 101-2221-E-007-090-MY3 and the National Tsing Hua University through Grant no. 102N2022E1. Y. L. Chueh greatly appreciates the use of facility at CNMM, National Tsing Hua University, through Grant no. 102N2744E1. This work is dedicated to the memory of Professor Li-Jen Chou at National Tsing Hua University, who passed away on December 14, 2012, before the completion of this work. Professor Chou has made significant contributions to nanoscience and engineering and will be missed and remembered as a caring mentor and an outstanding scientist.

References

[1] Y. L. Chueh, L. J. Chou, C. M. Hsu, and S. C. Kung, "Synthesis and characterization of taper- and rodlike Si nanowires on SixGe1-x substrate," *Journal of Physical Chemistry B*, vol. 109, no. 46, pp. 21831–21835, 2005.

[2] A. B. Greytak, C. J. Barrelet, Y. Li, and C. M. Lieber, "Semiconductor nanowire laser and nanowire waveguide electro-optic modulators," *Applied Physics Letters*, vol. 87, no. 15, Article ID 151103, 2005.

[3] C. S. Lao, J. Liu, P. Gao et al., "ZnO nanobelt/nanowire schottky diodes formed by dielectrophoresis alignment across au electrodes," *Nano Letters*, vol. 6, no. 2, pp. 263–266, 2006.

[4] Z. Zhong, D. Wang, Y. Cui, M. W. Bockrath, and C. H. Lieber, "Nanowire crossbar arrays as address decoders for integrated nanosystems," *Science*, vol. 302, no. 5649, pp. 1377–1379, 2003.

[5] R. F. Service, "Nanodevices make fresh strides toward reality," *Science*, vol. 302, no. 5649, p. 1310, 2003.

[6] P. Yang and C. M. Lieber, "Nanostructured high-temperature superconductors: creation of strong-pinning columnar defects in nanorod/superconductor composites," *Journal of Materials Research*, vol. 12, no. 11, pp. 2981–2996, 1997.

[7] M. H. Huang, S. Mao, H. Feick et al., "Room-temperature ultraviolet nanowire nanolasers," *Science*, vol. 292, no. 5523, pp. 1897–1899, 2001.

[8] Z. R. Dai, J. L. Gole, J. D. Stout, and Z. L. Wang, "Tin oxide nanowires, nanoribbons, and nanotubes," *Journal of Physical Chemistry B*, vol. 106, no. 6, pp. 1274–1279, 2002.

[9] X. S. Peng, Y. W. Wang, J. Zhang et al., "Large-scale synthesis of In_2O_3 nanowires," *Applied Physics A: Materials Science and Processing*, vol. 74, no. 3, pp. 437–439, 2002.

[10] Y. C. Choi, W. S. Kim, Y. S. Park et al., "Catalytic growth of β-Ga_2O_3 nanowires by arc discharge," *Advanced Materials*, vol. 12, pp. 746–750, 2000.

[11] Y. B. Li, Y. Bando, D. Goldberg, and K. Kurashima, "WO_3 nanorods/nanobelts synthesized via physical vapor deposition process," *Chemical Physics Letters*, vol. 367, no. 1-2, pp. 214–218, 2003.

[12] H. Schulz, L. Mädler, S. E. Pratsinis, P. Burtscher, and N. Moszner, "Transparent nanocomposites of radiopaque, flame-made Ta_2O_5/SiO_2 particles in an acrylic matrix," *Advanced Functional Materials*, vol. 15, no. 5, pp. 830–837, 2005.

[13] A. M. Morales and C. M. Lieber, "A laser ablation method for the synthesis of crystalline semiconductor nanowires," *Science*, vol. 279, no. 5348, pp. 208–211, 1998.

[14] R.-Q. Zhang, Y. Lifshitz, and S.-T. Lee, "Oxide-assisted growth of semiconducting nanowires," *Advanced Materials*, vol. 15, no. 7-8, pp. 635–640, 2003.

[15] Q. Wei and C. M. Lieber, "Solution-based synthesis of magnesium oxide nanorods," in *Proceedings of the MRS Fall Meeting—Symposium F 'Nanophase and Nanocomposite Materials III'*, pp. 3–7, December 1999.

[16] T. J. Trentler, K. M. Hickman, S. C. Goel, A. M. Viano, P. C. Gibbons, and W. E. Buhro, "Solution-liquid-solid growth of crystalline III-V semiconductors: an analogy to vapor-liquid-solid growth," *Science*, vol. 270, no. 5243, pp. 1791–1794, 1995.

[17] H. J. Fan, W. Lee, R. Hauschild et al., "Template-assisted large-scale ordered arrays of ZnO pillars for optical and piezoelectric applications," *Small*, vol. 2, no. 4, pp. 561–568, 2006.

[18] P.-C. Chang, Z. Fan, W.-Y. Tseng, A. Rajagopal, and J. G. Lu, "B-Ga_2O_3 nanowires: synthesis, characterization, and p-channel field-effect transistor," *Applied Physics Letters*, vol. 87, no. 22, Article ID 222102, 2005.

[19] Z. Fan, D. Wang, P.-C. Chang, W.-Y. Tseng, and J. G. Lu, "ZnO nanowire field-effect transistor and oxygen sensing property," *Applied Physics Letters*, vol. 85, no. 24, pp. 5923–5925, 2004.

[20] Z. Fan, X. Wen, S. Yang, and J. G. Lua, "Controlled p- and n-type doping of Fe_2O_3 nanobelt field effect transistors," *Applied Physics Letters*, vol. 87, Article ID 013113, 2005.

[21] H. Ohkubo, Y. Ohtera, S. Kawakami, and T. Chiba, "Design and fabrication of multichannel photonic crystal wavelength filters to suppress crosstalk of arrayed waveguide grating," *Japanese Journal of Applied Physics 1: Regular Papers and Short Notes and Review Papers*, vol. 44, no. 3, pp. 1534–1541, 2005.

[22] F. Rubio, J. Denis, J. M. Albella, and J. M. Martinez-Duart, "Sputtered Ta_2O_5 antireflection coatings for silicon solar cells," *Thin Solid Films*, vol. 90, no. 4, pp. 405–408, 1982.

[23] D. W. Graham and D. P. Stinton, "Development of tantalum pentoxide coatings by chemical vapor deposition," *Journal of the American Ceramic Society*, vol. 77, no. 9, pp. 2298–2304, 1994.

[24] H. Hara and T. Ohta, "Dynamic response of a Ta_2O_5-gate pH-sensitive field-effect transistor," *Sensors and Actuators, B: Chemical*, vol. 32, no. 2, pp. 115–119, 1996.

[25] D.-H. Kwona, B.-W. Cho, C.-S. Kim, and B.-K. Sohn, "Effects of heat treatment on Ta_2O_5 sensing membrane for low drift and high sensitivity pH-ISFET," *Sensors and Actuators, B: Chemical*, vol. 34, no. 1–3, pp. 441–445, 1996.

[26] T. Sreethawong, S. Ngamsinlapasathian, Y. Suzuki, and S. Yoshikawa, "Nanocrystalline mesoporous Ta_2O_5-based photocatalysts prepared by surfactant-assisted templating sol-gel process

for photocatalytic H_2 evolution," *Journal of Molecular Catalysis A: Chemical*, vol. 235, no. 1-2, pp. 1–11, 2005.

[27] A. Fukumoto and K. Miwa, "Prediction of hexagonal Ta_2O_5 structure by first-principles calculations," *Physical Review B—Condensed Matter and Materials Physics*, vol. 55, no. 17, pp. 11155–11160, 1997.

[28] C. J. Ballhausen, *An Introduction to Ligand Field Theory*, McGraw-Hill, New York, NY, USA, 1962.

[29] S. P. Murarka, "Refractory silicides for integrated circuits," *Journal of Vacuum Science & Technology*, vol. 17, no. 4, pp. 775–792, 1980.

[30] R. Beyers, "Thermodynamic considerations in refractory metal-silicon-oxygen systems," *Journal of Applied Physics*, vol. 56, no. 1, pp. 147–152, 1984.

[31] C. Milanese, V. Buscaglia, F. Maglia, and U. Anselmi-Tamburini, "Reactive growth of tantalum silicides in Ta-Si diffusion couples," *Journal of Physical Chemistry B*, vol. 106, no. 23, pp. 5859–5863, 2002.

[32] J. Szekely and N. Themelis, *Rate Phenomena in Process Metallurgy*, John Wiley & Sons, 1971.